THE JOURNAL OF PHYSICAL CHEMISTRY B

Article

pubs.acs.org/JPCB

Investigating the Structural Origin of Trpzip2 Temperature Dependent Unfolding Fluorescence Line Shape Based on a Markov State Model Simulation

Jian Song,[†,‡,#] Fang Gao,[§,#] Raymond Z. Cui,[∥] Feng Shuang,[§] Wanzhen Liang,[⊥] Xuhui Huang,[∥] and Wei Zhuang*[,†]

[†]State Key Lab of Molecular Reaction Dynamics, Dalian Institute of Chemical Physics, Dalian, 116023, China

[‡]College of Physics and Information Engineering, Henan Normal University, Xinxiang, Henan, 453007, China

[§]Institute of Intelligent Machines, Chinese Academy of Sciences, Hefei 230031, China

[∥]Department of Chemistry, Division of Biomedical Engineering, The Hong Kong University of Science and Technology, Clear Water Bay, Kowloon, Hong Kong

[⊥]Department of Chemistry, Xiamen University, Xiamen 316005, China

Supporting Information

ABSTRACT: Vibrationally resolved fluorescence spectra of the β-hairpin trpzip2 peptide at two temperatures as well as during a T-jump unfolding process are simulated on the basis of a combination of Markov state models and quantum chemistry schemes. The broad asymmetric spectral line shape feature is reproduced by considering the exciton−phonon couplings. The temperature dependent red shift observed in the experiment has been attributed to the state population changes of specific chromophores. Through further theoretical study, it is found that both the environment's electric field and the chromophores' geometry distortions are responsible for tryptophan fluorescence shift.

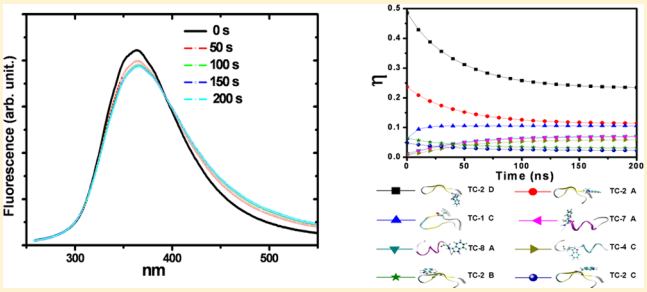

I. INTRODUCTION

Understanding the mechanism of protein folding is a significant task in life science.[1−10] The protein conformational changes are commonly monitored by the spectroscopic tools including infrared spectroscopy, circular dichroism, and fluorescence.[11−16] Among these, fluorescence spectroscopy remains one of the most successful tools for understanding the protein folding. The changes of fluorescence wavelength, intensity, line shape, and lifetime of the intrinsic or extrinsic fluorophores are monitored and assigned to different folding stages.[17,18] Further unraveling of the fluorescence signals with more molecular level insight usually requires the help from theoretical modeling,[19−22] which is in general complicated due to the entangled and congested nature of the fluorescence transitions as well as the difficulties in simulating the protein folding processes.

The hybrid quantum mechanics and molecular mechanics (QM/MM) method is commonly used to model the fluorescence line shape in the protein−solvent systems.[23−26] Many models can be employed to count in the vibrational feature of the fluorescence spectra for single chromophores, such as the Brownian oscillator model,[27−31] the displaced harmonic oscillator model,[32] and the anharmonic oscillator model.[33−35] For the multichromophoric systems with weak couplings between the units, one can adopt the Frenkel exciton model[36−40] for the Hamiltonian construction, which is widely used in the optical response calculation of biological system.[41−45]

The nontrivial work required in sampling the configuration distribution and long time scale folding kinetics[46−48] adds an extra layer of complexity in simulating the peptide folding fluorescence. In a recent work, we proposed a Markov state model (MSM)[49] based protocol to simulate the linear and nonlinear peptide infrared spectra at two temperatures, at which the peptide is in different folding status. We also simulated the long time scale T-jump peptide unfolding and the related transient vibrational spectra. We applied the method on a β-hairpin peptide trpzip2, whose folding thermodynamics and kinetics have been investigated extensively.[17,18,50,51]

In this paper, we adopted a similar approach to simulate the vibrationally resolved tryptophan band line shape of trpzip2's fluorescence spectrum based on the MSMs. We first present our model with a description of the parameters and computational details. Then we conclude with a discussion and analysis of the results.

Received: May 15, 2012
Revised: September 19, 2012
Published: September 20, 2012

II. SYSTEM AND METHODS

MSMs decompose conformational space into a set of metastable states with fast intrastate but slow interstate transitions.[52−56] The resulting discrete state MSMs are Markovian at a discrete unit of time Δt, under the condition that Δt is longer than the intrastate relaxation time. In another word, the probability for the system to visit a given state at time $t + \Delta t$ only depends on the state it visited at time t. This allows MSMs constructed many short simulations to model the global long time scale dynamics by

$$\mathcal{P}(n\Delta t) = [\mathcal{T}(\Delta t)]^n \mathcal{P}(0) \tag{1}$$

where $\mathcal{P}(n\Delta t)$ is a vector of state populations at time $n(\Delta t)$, $\mathcal{T}$ is the column stochastic transition probability matrix, and the element of this matrix P_{ji} denotes the probability of observing the system in state j at time t given that it was previously observed in state i at time $t - (\Delta t)$. (Δt), the time interval to count the transitions, is the lag time, also called τ. In this work, we adopted MSMs built in our previous work[49] to model the T-jump unfolding dynamics of the trpzip2 peptide. In particular, we have first constructed 17-state MSMs at 300 K and 13-state MSMs at 350 K after the T-jump. Because it is obviously too expensive to calculate spectral contributions of all the conformations for all the metastates from MD simulation, we examine the fluorescence contributions for one typical folded metastate and one typical unfolded metastate. In each state we pick two configurations: the most probable typical conformation (TC) and a configuration randomly selected from the top 10 highest probable configurations besides the typical conformation, which is named random conformation (RC). We compared spectral line shapes of these four comformations and found conformations within the same metastable state have relatively similar line shapes (the spectra and details can be found in the Supporting Information). So we have then computed the fluorescence spectra for each metastable state from its representative conformations. To obtain the overall fluorescence signal, we simply sum over spectra of different metastable states weighted by their populations.

In the current study, the tryptophan band is described by an effective Hamiltonian, in which the ground state Hamiltonian is

$$H^{\mathrm{g}}(x_1,...,x_p) = |0\rangle[\sum_{n=1}^{p} h_n^0(x_n)]\langle 0| \tag{2}$$

Here p is the index for the tryptophan chromophores and h_n^0 is the ground state Hamiltonian of monomer n. The adjacent excited state configurations interact via coupling elements J, and the excited state nuclear Hamiltonian is a $p \times p$ matrix of the form

$$H^{\mathrm{e}}(x_1,...,x_p) = \begin{pmatrix} h_1^{\mathrm{e}} & J_{1,2} & \cdots & \cdots & J_{1,p} \\ J_{1,2} & h_2^{\mathrm{e}} & \cdots & \cdots & J_{2,p} \\ \cdots & \cdots & \cdots & \cdots & \cdots \\ J_{1,p-1} & J_{2,p-1} & \cdots & h_{p-1}^{\mathrm{e}} & J_{p-1,p} \\ J_{1,p} & J_{2,p} & \cdots & J_{p-1,p} & h_p^{\mathrm{e}} \end{pmatrix} \tag{3}$$

where h_n^{e} represents the excited state Hamiltonian of the nth monomer and $J_{m,n}$ is the coupling between two Frenkel exciton (FE) states localized on the monomers m and n.

In the framework of time-dependent density functional theory, Hsu et al. derived an expression for energy transfer coupling by considering the energy splitting of the chromophores from their excited states.[57] With the first-order approximation, J is split into the following three terms as

$$J_{m,n} = J_{m,n}^{\mathrm{coul}} + J_{m,n}^{\mathrm{ex}} + J_{m,n}^{\mathrm{overlap}} \tag{4}$$

where $J_{m,n}^{\mathrm{coul}}$, $J_{m,n}^{ex}$, and $J_{m,n}^{\mathrm{overlap}}$ are defined as

$$J_{m,n}^{\mathrm{coul}} = \int \mathrm{d}r \int \mathrm{d}r'\, \rho_m^1(r) \frac{1}{|r - r'|} \rho_n^1(r'),$$
$$J_{m,n}^{\mathrm{ex}} = \int \mathrm{d}r \int \mathrm{d}r'\, \rho_m^1(r)\, g_{\mathrm{XC}}(r,r',\omega_0)\, \rho_n^1(r') \tag{5}$$

For a molecular dimer, $J_{m,n}^{\mathrm{overlap}} = -\omega_0 \int \mathrm{d}r\, \rho_m^1(r)\, \rho_n^1(r)$. Here ω_0 is the transition frequency and ρ_m^1 and ρ_n^1 are the transition densities of the first excited state of molecule m and n, respectively.

In the above Frenkel exciton model, the ground state and the excited state Hamiltonians of each monomer can be written, respectively, as

$$h_m^0 = -\frac{1}{2}\frac{\mathrm{d}^2}{\mathrm{d}x^2} + \frac{1}{2}\omega_0{}^2 x^2 \tag{6}$$

$$h_m^{\mathrm{e}} = -\frac{1}{2}\frac{\mathrm{d}^2}{\mathrm{d}x^2} + \frac{1}{2}\omega_0{}^2 (x - x_{\mathrm{e}})^2 + \Delta E_{\mathrm{FE}} \tag{7}$$

x is the coordinate, and ΔE_{FE} is the 0−0 transition energy. x_{e} and ω_0 are the effective displacement and frequency, respectively. In the observed spectra of dissolved chromophores,[17] the internal vibrations are not obviously resolved. Due to the large Gaussian broadening arising from a fluctuating shell of surrounding solvent molecules, they merge into a single vibronic progression. Considering the computational cost, the effective mode approximation is usually adopted in calculation of the spectra of aggregates.[58−61] Generally, there are two ways to obtain the effective mode. One way is to employ ab initio or first-principle calculations, and the other is to fit the mode with the experimental data. We have adopted the first way, that is, the procedure in ref 62, to calculate the spectra of perylene bisimide oligomers[38] and rubrene multichromophores[58] in our previous works. Spano et al.[59,60] and Engel et al.[61] directly assigned a value to the effective mode according to the experiment. Both these two ways employed the approximation of one effective mode, which showed good performance in practice. Here the effective mode can be described with Huang−Rhys factor,[62]

$$S = \frac{\lambda}{\omega_0} = \frac{\sum_k \lambda_k}{\omega_0} \tag{8}$$

$$\omega_0 = \sqrt{\frac{\sum_k \omega_k{}^4 x_{\mathrm{e}(k)}{}^2}{\sum_k \omega_k{}^2 x_{\mathrm{e}(k)}{}^2}} \tag{9}$$

The effective displacement x_{e} is related to S by $S = {}^1/_2 \omega_0 x_{\mathrm{e}}{}^2$. The reorganization energy λ_k of each mode ω_k is $\lambda_k = s_k \omega_k$ and the Huang−Rhys factor s_k for each mode ω_k can also be expressed in terms of the displacement parameter $x_{e(k)}$ as $S_k = {}^1/_2 \omega_k x_{\mathrm{e}(k)}{}^2$. With the constructed Hamiltonians H^{g} and H^{e} above, the correlation function $C_{\mathrm{e}}(t)$ for emission in linear response spectroscopy is given as

$$C^e(t) = \frac{\mathrm{Tr}[e^{-\beta H^e} e^{iH^e t/\hbar} \mu e^{-iH^g t/\hbar} \mu]}{\mathrm{Tr}[e^{-\beta H^e}]} \quad (10)$$

Thus, the optical emission cross section $\beta(\omega)$ can be obtained

$$\beta(\omega) \propto \omega^3 \int_{-\infty}^{\infty} dt \exp(-i\omega t - \gamma|t|) C^e(t) \quad (11)$$

Here γ represents the dephasing factor. In current work, we directly obtain the fluorescence spectra in the frequency domain. We get the eigen ground and excited vibronic states by diagonalizing the aggregate ground and excited state Hamiltonians. The exciton−phonon couplings just modulate the overlap integrals between the ground and excited vibronic states of the monomers, which are employed to calculate the transition probability from the excited vibronic states to the ground vibronic states of the aggregate. Then we assume the Gaussian form for the damping-induced broadening in the fluorescence spectra, and the full width at half maximum (FWHM) is set to be 0.3 eV to have a best fit of the experimental line shape.

All the parameters of Hamiltonian are calculated by quantum chemistry based on the representative trpzip2 conformations obtained from previously constructed MSMs.[49] In ref 49, 17-state and 13-state MSMs have been built from extensive molecular dynamic simulations at 300 and 350 K, respectively. In the current study, we have selected one representative conformation from each metastable state for the further calculation of the fluorescence signal. The representative conformation has been chosen as the central conformation of the most probable microstate (see ref 49 for details of the microstate construction) within each metastable state. For simplicity, here we use TC-n (typical conformation n) to label the representative conformation of each mestable state, for example, TC-2 is the typical structure for metastable state 2. A QM/MM protocol is adopted for site energy calculation of each tryptophan chromophore. Specifically, the 3-methylindole (3MI) moiety of tryptophan is selected as the inner part (Figure 1), the rest part of the protein is the middle part, and all

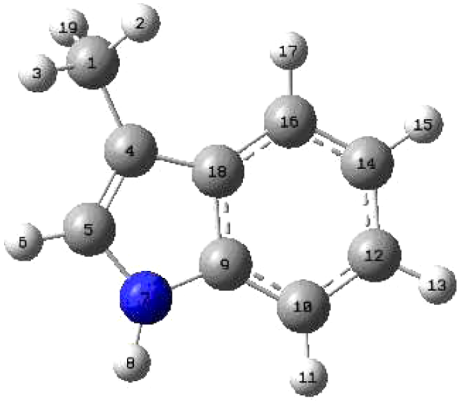

Figure 1. 3-Methyl indole (3MI) structure with the atom indices.

the water molecules are the outer part. The broken bond between inner and middle layer is hydrogen saturated. The ground state geometry optimization and frequency analysis for each chromophore were performed using DFT/AM1/AMBER method.[63] The equilibrium geometry of ^1L_a, the excited state responsible for the emission, was optimized at TD-DFT/AM1/AMBER level. We adopted the approximation that the excited state frequencies equals those of ground state due to the computational cost. The basis set is 3-21g and the AMBER force field consists with what was used in the MD simulation. All the QM/MM calculations were carried out using Gaussion09[64] software, except that the exciton−exciton couplings $J_{m,n}$ were calculated using Equation4 within a developed version of Q-Chem software.[65]

A good description of ^1L_a is important for the fluorescence calculation. Several functionals, such as B3LYP[66] and LRC functionals[67,68](wB97X and LC-BLYP), were adopted to calculate the electronic structures of 3MI both in a vacuum and in water. The CASSCF/CASPT2 calculation,[69] which is considered to be the most accurate protocol for the tryptophan excited states modeling,[70] was also carried out as a benchmarking reference. The calculated energies of the first two excited states ^1L_a and ^1L_b with different methods are listed in Table 1 in the Supporting Information. Compared with the transition to ^1L_b, the transition between the ground and ^1L_a state has a sizable charge transfer component from the pyrrole ring to the benzene ring and the two states can be distinguished between each other by the transition molecular orbital components and the transition intensities, etc. The transition energies of ^1L_a in B3LYP functional and CASSCF/CASPT2 agree better with the experiment (details can be found in the Supporting Information), in spite of reorder occurrence between the two states in B3LYP result. Considering the computational cost, in the following calculation, we adopted the B3LYP/TD-B3LYP protocol to model the 3MI fluorophores.

III. RESULTS AND DISCUSSION

Using the protocol introduced above, one can obtain the vibrationally resolved fluorescence spectra of trpzip2 by summing the weighted contributions from different conformers, which are generated from the simulation database by MSMs. The simulated equilibrium populations of each states at 300 and 350 K were published in ref 49.

Figure 2 presents the steady state spectra at 300 K, which nicely resemble the experimental line shape in ref 17. The maximum of the simulated fluorescence is ∼332.6 nm (the black line in Figure 2) whereas that of the experimental trpzip2 fluorescence is ∼351 nm at 297 K.[17] Consistent with the

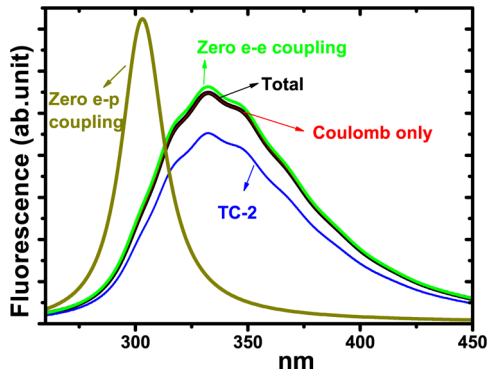

Figure 2. Calculated fluorescence spectra of trpzip2 at 300 K. The black curve is the overall fluorescence spectrum; the blue curve corresponds to the contribution from metastable state 2; the red curve is calculated with only the Coulomb term considered in the exciton−exciton couplings; the bright green curve is calculated with zero exciton−exciton coupling; the light gray is calculated with no exciton−phonon coupling.

dx.doi.org/10.1021/jp304714q | J. Phys. Chem. B 2012, 116, 12669−12676

experiment, the simulated spectrum shows a significant asymmetric feature. To quantify this, we calculated the unsymmetrical ratio between the right part and the left part of FWHM. This ratio has a value of ~1.68 at 300 K, whereas the experimental value at 297 K is about 1.57.[17] The line shape of the spectra at 350 K become more asymmetric, as demonstrated in Figure 3, with a unsymmetrical ratio of

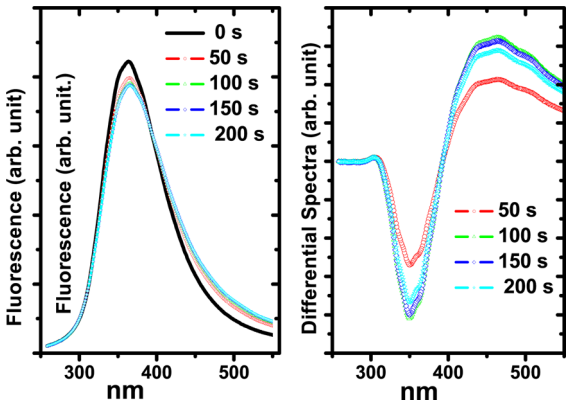

Figure 3. *T*-jump induced transient fluorescence lineshapes (left) and the differential spectra (right) between 0 and 200 ns.

~1.71. The experimental[17] ratio at 347 K is about 1.88. A 3.4 nm red shift is found between the simulated 300 and 350 K fluorescence signals. This agrees with Gruebele's experiment, in which they reported a 3–5 nm red shift from 297 to 347 K.[17] Our simulation thus decently reproduced the experimental tryptophan band fluorescence signal and its temperature dependence.

To understand the microscopic origin of the asymmetric line shape, we first examined the spectral contributions of the TC-states, which are all asymmetric and have only slightly smaller unsymmetrical ratios compared with those of the overall feature. As an example, the spectral contribution from the folded TC-states, which has the largest population at 300 K, is plotted in Figure 2. And its unsymmetrical ratio is 1.33. We also calculated the fluorescence with no exciton–phonon couplings, and the resulting spectrum, which is the light gray curve in Figure 2, has a perfectly symmetric feature. Due to the exciton–phonon coupling, the potential energy surfaces of the ^1L_a electronic state and ground state do not keep same shape appearance and location, and then normal coordinate displacements between them emerge. As a result, the fluorescence spectra show asymmetric line shape. It should be noted that in the manuscript, we set the effective displacement of our procedure to be zero to demonstrate no exciton–phonon coupling case. It can be conclued that the asymmetric feature observed in the fluorescence mainly originates from the vibronic couplings instead of the conformational inhomogeneity.

We also studied the effect of the exciton–exciton couplings on the line shape. The red line in Figure 2 is calculated with only the first coulomb term of the exciton–exciton couplings considered, and the bright green line is the calculated spectrum with no exciton coupling. Compared with the original black curve, these two curves only have minor changes. The ^1L_a states are thus largely localized on the tryptophan groups. We indexed these four localized states for each trpzip2 configuration as A–D. The locations of these states on the peptide are shown in the Supporting Information.

A temperature jump induced fluorescence signal was also simulated using the same protocol as in ref 49, the populations of metastable states will relax to the equilibrium distribution at T_2 starting from their initial distributions. On the basis of the population relaxation of each metastable state, the transient fluorescence signals at different moments can be generated. The population change converges at about 200 ns. The line shape of the spectrum during the *T*-jump process (Figure 3) also has the asymmetric character. At 0 ns, the spectral maximum is 350.6 nm, with unsymmetrical ratio about 1.51. From 0 to 200 ns, the spectral maximum gradually red shifts and the asymmetricity increases. The differential spectra from 0 ns are also plotted in Figure 3. Compared with 0 ns, the

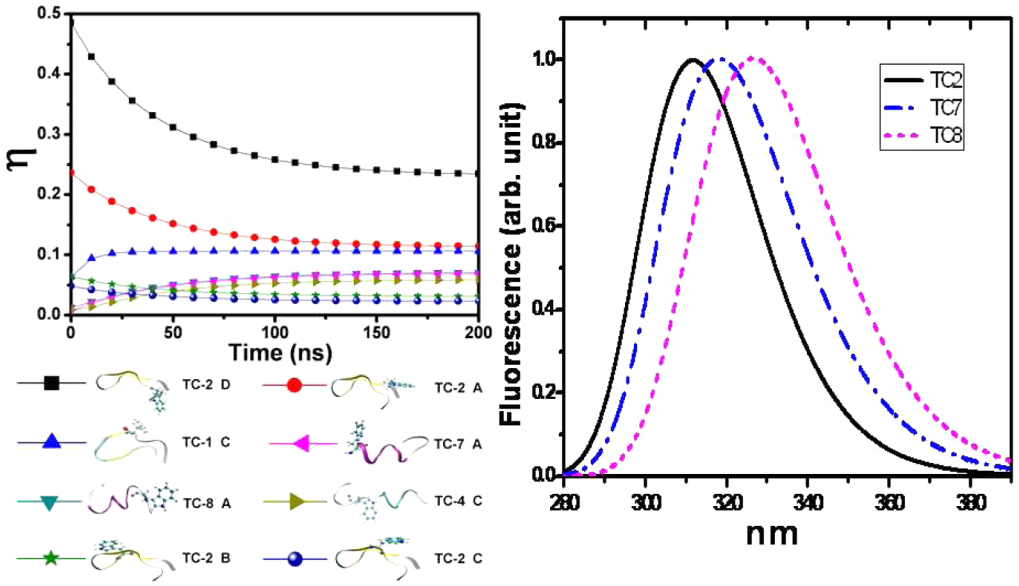

Figure 4. Time dependence of the state population weights η after the *T*-jump (top) and the conformations of the tryptophan fluorophores on which the 8 most populated ^1L_a states located (bottom). On the right, one typical folded state and two typical unfolded states' fluorescence spectra are showed.

dx.doi.org/10.1021/jp304714q | J. Phys. Chem. B 2012, 116, 12669–12676

intensity of blue tail decreases and that of red tail increases. As we discussed in ref 49, a temperature jump of 10−20 K is usually used in a *T*-jump experiment, and we adopted a 50 K jump here simply to induce more significant structural changes. More discussion on this issue and also on *T*-jump study of Trpzip2 can be found in ref 49.

To reveal the molecular details underlying the trpzip2 unfolding fluorescence, we define $\eta_{ir} = \mathcal{P}_i\mathcal{B}_{ir}$ for a specific ^1L_a state r (r = A, B, C, D) in a peptide conformation TC-state *i*. Here, $\mathcal{P}_i$ is the TC-state population in eq 1, and $\mathcal{B}_{ir} = e^{-E_{ir}/kT}/\Sigma_{r'}e^{-E_{ir'}/kT}$ is the Boltzmann weight of the ^1L_a state with index r (r = A, B, C, D); E_{ir} is the corresponding excitation energy. η_{ir} thus represents the probability of a certain state *ir* as the initial state of the emission. Changes of η for all the 52 states during the *T*-jump unfolding process are plotted in the top panel of Figure 4. The locations of the eight most weighted fluorophores are demonstrated at the bottom panel of Figure 4. The two fluorophores with largest η are both on the TC2, a typical folded state. When the temperature changes from 300 to 350 K, η decrease from 48.5% to 23.1% for TC-2 D and from 23.6% to 11.3% for TC-2 A, respectively. And the values for TC-1 C, TC-8 A, and TC-7 A increase from 6.3%, 1.3%, and 0.8% to 10.6%, 7.2%, and 7.0%, respectively. We can also define $\alpha_{ir} = \eta_{ir}D_{ir}^2$, in which D_{ir} is the amplitude of the transition dipoles. α thus represents the contribution of a certain state to the spectrum. The variations of α are very similar to η (see the Supporting Information). The excitation energies of these states are given in Table 1. Most of the fluorophores on the unfolded configurations, including 1C, 8A, 7A, and 4C have significant red-shifted transition energies compared with those on the folded configurations, such as 2D and 2A. The analysis above provides a molecular level explanation of the fluorescence change with the rise of temperature: As the temperature increases, the trpzip2 peptide experiences an unfolding process, the populations of blue-end fluorophores on the folded peptides, such as TC-2 D and TC-2 A, decrease and those of red-end fluorophores on the unfolded peptides, such as TC-8 A and TC-7 A, increase at the same time, which causes the red shift in the spectrum.

Table 1. Vertical Excitation Energies (nm) of the First Eight Largest Contributed 3MI Fluorophores Calculated with the Three-Layer ONIOM Method

2D	2A	1C	8A	7A	4C	2B	2C
309.4	307.8	316.2	316.3	322.8	314.3	304.8	304.1

To explore the structural origin of the observed transition frequency variations of the eight most weighted fluorophores, their excited state equilibrium geometries were generated. Different from a single 3MI in vacuum, which has a coplanar indole ring for ^1L_a, those fluorophores all have more or less distorted indole ring conformations, which is demonstrated by the dihedral angles listed in Table 2. We chose the dihedral angle 4−18−9−10 to reflect the extent of distortion between the benzene and pyrrole groups in the indole ring and for the eight fluorophores, and none of these angles is 180°. The dihedral angle 4−18−9−7 and 16−18−9−10 represent the twisting character of the pyrrole ring and benzene ring, respectively. Neither is flat.

To understand the influence of the environment on the tryptophan fluorescence, we investigated the correlation between the tryptophan transition frequencies and the environmental factors. Calculations are performed on ^1L_a equilibrium states of all 52 3MIs at 350 K. On the basis of a three-layer ONIOM model[71] of each 3MI, we calculated the Mulliken population with AM1 for atoms in the second layer, the charges of water molecules were taken from the AMBER force field. We then calculated the electric potential on each of the 10 heavy atoms in 3MI generated by the point charge distribution of the environment. On the basis of those 52 calculated data sets, we fitted the 3MI transition energy with 10 parameters using multiple linear regression analysis. The left panel of Figure 5 shows the poor correlation between the fitted transition energies and the transition energies calculated by quantum chemistry. The ^1L_a state of tryptophan fluorophores is a typical $\pi-\pi^*$ conjugated transition on the indole ring. Thus the geometry distortion of the 3MI group, which is induced by the environment and has an effect on the electronic delocalization, may have influence on the transition energy as well. We thus carried out another fitting procedure that includes six geometry parameters to describe the mechanical influence of the environment on the transition frequencies (One can find the parameter definition details in the Supporting Information.) The middle part of Figure 5 gives a better correlation between geometry parameters and transition energies. And then the right part of Figure 5, which includes both environmental electric potential and environment induced geometry changes and shows the more largely improved correlation between the fitted and calculated transition energy. A further construction of the quantitative relationship between

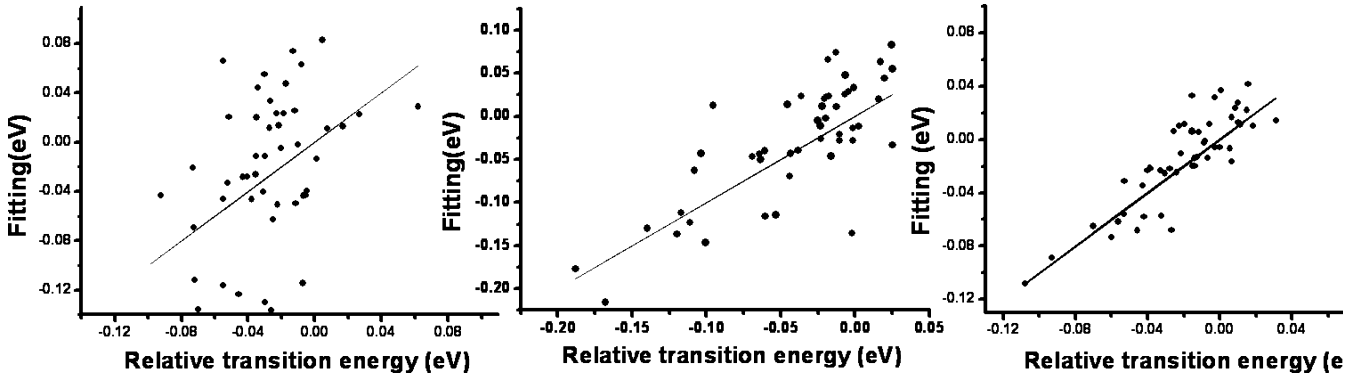

Figure 5. Correlations between the electric potentials and the transition energies only (left), between geometry parameters and the transition energies only (middle), and between electric potentials plus geometry parameters and the transition energies (right).

dx.doi.org/10.1021/jp304714q | J. Phys. Chem. B 2012, 116, 12669−12676

Table 2. Dihedral Angles (deg) for the Eight Geometries with the Atoms Labeled the Same as in Figure 1

dihedral angle	2D	2A	1C	8A	7A	4C	2B	2C
1−4−5−7	165.8	170.3	175.9	167.6	152.2	165.2	178.6	175.1
4−18−9−7	5.9	3.7	2.3	0.2	3.8	2.8	3.9	2.1
4−18−9−10	171.6	175.3	176.1	173.6	167.0	170.4	176.7	175.2
16−18−9−10	3.7	3.3	2.4	2.0	1.0	0.9	3.5	1.0

the transition frequencies and the environment requires a much more thorough and delicate consideration of both the electric field and the geometrical factors, related investigation is undergoing and beyond the scope of current manuscript.

In summary, we have simulated the equilibrium vibrationally resolved fluorescence of a β-hairpin trpzip2 peptide and its relaxation dynamics upon the laser induced T-jump. To achieve this, we have integrated MSMs to sample the equilibrium configuration distribution and to model the unfolding dynamics. A quantum chemistry protocol is then used to compute the fluorescence signal. We attribute the asymmetrical fluorescence line shape observed in the experiment mostly to the exciton−phonon coupling instead of the structural inhomogeneity. With increasing temperature, the populations of high frequency transitions in the folded conformers decrease while low frequency transitions in the unfolded conformers increase, which not only leads to FWHM change of spectral line shape but also induces a red shift in fluorescence maximum. Further investigation on the origin of tryptophan fluorescence suggests a combined influence from both the environment field and the 3MI geometry distortion.

■ ASSOCIATED CONTENT

Supporting Information

Structure of the central 3-MI unit and related benchmark calculation results, frontier orbitals of 3-MI, fluorescence contributions of configurations and fluorescence spectra for metastates 2 and 7, total population states (η and α vs time), conformations of 3-MI fluorophores and of tryptophans in TC-2, and structural parameters used in the article. Complete refs 64 and 65. This information is available free of charge via the Internet at http://pubs.acs.org

■ AUTHOR INFORMATION

Corresponding Author

*E-mail: W.Z., wzhuang@dicp.ac.cn

Notes

The authors declare no competing financial interest.

[#]J.S. and F.G. are co-first-authors.

■ ACKNOWLEDGMENTS

W.Z. gratefully acknowledges the support of the NSFC QingNian Grant 21003117, NSFC Key Grant 21033008 and Instrument in Science and Technological Ministry of China Grant 2011YQ09000505. J.S. acknowledges the support of the NSFC QingNian Grant 21103166. W.Z.L. is thankful for the financial support from the National Basic Research Program of China (Grant No.2011CB808501). F.G. and F.S. acknowledge the suppport from NSFC QingNian Grant 61203061 and NSFC Grant 61074052. X.H. acknowledges the support from the Hong Kong Research Grant Council HKUST2/CRF/10 and DAG09/10.SC03. We thank Dr. Z. L. Zheng and M. S. G. X. Sun for assistance with CASSCF/CASPT2 calculation.

■ REFERENCES

(1) Anfinsen, C. B. Principles that Govern Folding of Protein Chains. *Science* **1973**, *181*, 223−230.

(2) Nicholls, A.; Sharp, K. A.; Honig, B. Protein Folding and Association: Insights from the Interfacial and Thermodynamic Properties of Hydrocarbons. *Proteins* **1991**, *11*, 281−296.

(3) Gething, M. J.; Sambrook, J. Protein Folding in the Cell. *Nature* **1992**, *355*, 33−45.

(4) Wolynes, P. G.; Onuchic, J. N.; Thirumalai, D. Navigating the Folding Routes. *Science* **1995**, *267*, 1619−1620.

(5) Dill, K. A.; Bromberg, S.; Yue, K.; Fiebig, K. M.; Yee, D. P.; Thomas, P. D.; Chan, H. S. Principles of Protein-folding - a Perspective from Simple Exact Models. *Science* **1995**, *4*, 561−602.

(6) Onuchic, J. N.; Luthey-Schulten, Z.; Wolynes, P. G. Theory of Protein Folding: The Energy Landscape Perspective. *Annu. Rev. Phys. Chem.* **1997**, *48*, 545−600.

(7) Onuchic, J. N.; Nymeyer, H.; Garcia, A. E.; Chahine, J.; Socci, N. D. The Energy Landscape Theory of Protein Folding: Insights into Folding Mechanisms and Scenarios. *Adv. Protein Chem.* **2000**, *53*, 87−152.

(8) Dobson, C. M. Protein Folding and Misfolding. *Nature* **2003**, *426*, 884−890.

(9) Thirumalai, D.; O'Brien, E. P.; Morrison, G.; Hyeon, C. Theoretical Perspectives on Protein Folding. *Annu. Rev. Biophys.* **2010**, *39*, 159−183.

(10) Korzhnev, D. M.; Religa, T. L.; Banachewicz, W.; Fersht, A. R.; Kay, L. E. A Transient and Low-Populated Protein-Folding Intermediate at Atomic Resolution. *Science* **2010**, *329*, 1312−1316.

(11) Righetti, P. G.; Verzola, B. Folding/Unfolding/Refolding of Proteins: Present Methodologies in Comparison with Capillary Zone Electrophoresis. *Electrophoresis* **2001**, *22*, 2359−2374.

(12) Cai, X. M.; Dass, C. Conformational analysis of proteins and peptides. *Curr. Org. Chem.* **2003**, *7*, 1841−1854.

(13) Vass, E.; Hollosi, M.; Besson, F.; Buchet, R. Vibrational Spectroscopic Detection of Beta- and Gamma-turns in Synthetic and Natural Peptides and Proteins. *Chem. Rev.* **2003**, *103*, 1917−1954.

(14) Uversky, V. N.; Fink, A. L. Conformational Constraints for Amyloid Fibrillation: The Importance of Being Unfolded. *Biochim. Biophys. Acta* **2004**, *1698*, 131−153.

(15) Receveur-Brechot, V.; Bourhis, J. M.; Uversky, V. N.; Conrad, B.; Longhi, S. Assessing Protein Disorder and Induced Folding. *Proteins* **2006**, *62*, 24−45.

(16) Cui, R. Z.; Silva, D. A.; Song, J.; Bowman, G. R.; Zhuang, W.; Huang, X. Bridging the Gap Between Optical Spectroscopic Experiments and Computer Simulations for Fast Protein Folding Dynamics. *Curr. Phys. Chem.* **2012**, *2*, 45−58.

(17) Yang, W. Y.; Pitera, J. W.; Swope, W. C.; Gruebele, M. Heterogeneous Folding of the Trpzip Hairpin: Full Atom Simulation and Experiment. *J. Mol. Biol.* **2004**, *336*, 241−251.

(18) Yang, W. Y.; Gruebele, M. Detection-dependent Kinetics as a Probe of Folding Landscape Microstructure. *J. Am. Chem. Soc.* **2004**, *126*, 7758−7759.

(19) Kim, J.; Kapitaán, J.; Lakhani, A.; Bouř, P.; Keiderling, T. A. Tight β-turns in Peptides. DFT-based Study of Infrared Absorption and Vibrational Circular Dichroism for Various Conformers Including Solvent Effects. *Theor. Chem. Acc.* **2008**, *119*, 81−97.

(20) Roy, S.; Jansen, T. L. C.; Knoester, J. Structural Classification of the Amide I Sites of a Beta-hairpin with Isotope Label 2DIR Spectroscopy. *Phys. Chem. Chem. Phys.* **2010**, *12*, 9347−9357.

(21) Bahar, I.; Lezon, T. R.; Yang, L. W.; Eyal, E. Global Dynamics of Proteins: Bridging Between Structure and Function. *Annu. Rev. Biophys.* **2010**, *39*, 23−42.
(22) Skjaerven, L.; Reuter, N.; Martinez, A. Dynamics, Flexibility and Ligand-induced Conformational Changes in Biological Macromolecules: A Computational Approach. *Future. Med. Chem.* **2011**, *3*, 2079−2100.
(23) Senn, H. M.; Thiel, W. QM/MM Methods for Biomolecular Systems. *Angew. Chem., Int. Ed. Engl.* **2009**, *48*, 1198−1229.
(24) Friesner, R. A.; Guallar, V. Ab initio Quantum Chemical and Mixed Quantum Mechanics/Molecular Mechanics (QM/MM) Methods for Studying Enzymatic Catalysis. *Annu. Rev. Phys. Chem.* **2005**, *56*, 389−427.
(25) Vivian, J. T.; Callis, P. R. Machanisms of Tryptophan Fluorescence Shifts in Proteins. *Biophys. J.* **2001**, *80*, 2093−2109.
(26) Onuchic, J. N.; Wolynes, P. G. Theory of Protein Folding. *Curr. Opin. Struc. Biol.* **2004**, *14*, 70−75.
(27) Mukamel, S.; Tanimura, Y. Two-Dimensional Femtosecond Vibrational Spectroscopy of Liquids. *J. Chem. Phys.* **1993**, *99*, 9496.
(28) Mukamel, S. *Principles of Nonlinear Optical Spectroscopy*; Oxford University Press: Oxford, U.K., 1995; pp 226−234.
(29) Kato, T.; Tanimura, Y. Two-dimensional Raman and Infrared Vibrational Spectroscopy for a Harmonic Oscillator System Nonlinearly Coupled with a Colored Noise Bath. *J. Chem. Phys.* **2004**, *120*, 260.
(30) Zhao, Y.; Knox, R. S. A Brownian Oscillator Approach to the Kennard-Stepanov Relation. *J. Phys. Chem. A* **2000**, *104*, 7751−7761.
(31) Shi, S. L.; Li, G. Q.; Xu, S. J.; Zhao, Y.; Chen, G. H. Green luminescence Band in ZnO: Fine Structures, Electron-phonon Coupling, and Temperature Effect. *J. Phys. Chem. B* **2006**, *110*, 10475−10478.
(32) Yan, Y. J.; Mukamel, S. Eigenstate-free, Green function, Calculation of Molecular Absorption and Fluorescence Line Shapes. *J. Chem. Phys.* **1986**, *85*, 5908−5923.
(33) Song, J.; Liang, W. Z.; Zhao, Y.; Yang, J. L. Conformational Flexibility and its Effect on the Vibrationally Resolved Absorption and Fluorescence Spectra of Oligofluorenes. *Appl. Phys. Lett.* **2006**, *89*, 071917.
(34) Gao, F.; Zhao, Y.; Liang, W. Z. Theoretical Studies Toward Understanding the Excited State Dynamics of a Bichromophoric Molecule. *J. Chem. Phys.* **2007**, *126*, 2224509.
(35) Liang, W. Z.; Zhao, Y.; Sun, J.; Song, J.; Hu, S. L.; Yang, J. L. Electronic excitation of polyfluorenes: A theoretical study. *J. Phys. Chem. B* **2006**, *110*, 9908−9915.
(36) Gelzinis, A.; Abramavicius, D.; Valkunas, L. Non-Markovian Effects in Time-resolved Fluorescence Spectrum of Molecular Aggregates: Tracing Polaron Formation. *Phys. Rev. B* **2011**, *84*, 245430.
(37) Gao, F.; Liang, W. Z.; Zhao, Y. Theoretical Studies of Vibrationally Resolved Absorption and Emission Spectra: From a Single Chromophore to Multichromophoric Oligomers/Aggregates. *Sci. China Chem.* **2010**, *53*, 297−309.
(38) Gao, F; Liang, W. Z.; Zhao, Y. Vibrationally Resolved Absorption and Emission Spectra of Rubrene Multichromophores: Temperature and Aggregation Effects. *J. Phys. Chem. A* **2009**, *113*, 12847−12856.
(39) Frenkel, J. On the Transformation of Light into Heat in Solids. *Phys. Rev.* **1931**, *37*, 17−44.
(40) Davydov, A. S. *Theory of Molecular Excitons*; Plenum Press: New York, 1971.
(41) Abramavicius, D.; Mukamel, S. Quartic Interband Exciton Couplings in Pump-probe Spectroscopy of Light Harvesting Complexes. *J. Phys. Chem. B* **2004**, *108*, 10295.
(42) Renger, T. H.; Marcus, R. A. On the Relation of Protein Dynamics and Exciton Relaxation: An Estimation of the Spectral Density and a Theory for the Calculation of Optical Spectra. *J. Chem. Phys.* **2002**, *116*, 9997−10019.
(43) Song, J.; Gao, F.; Liang, W. Z. How does the Nonlocal HF Exchange Influence the Electron Excitation of Bacteriochlorophyll and its Assembly. *Comput. Theor. Chem.* **2011**, *965*, 53−59.
(44) Ohta, K.; Yang, M.; Fleming, G. R. Ultrafast Exciton Dynamics of J-aggregates in Room Temperature Solution Studied by Third-order Nonlinear Optical Spectroscopy and Numerical Simulation based on Exciton Theory. *J. Chem. Phys.* **2001**, *115*, 7609−7621.
(45) Zhang, W. M.; Meier, T.; Chernyak, V; Mukamel, S. Simulation of Three-pulse-echo and Fluorescence Depolarization in Photosynthetic Aggregates. *Philos. Trans. R. Soc. London A* **1998**, *356*, 405−419.
(46) Khorvash, M.; Lamour, G.; Gsponer, J. Long-time Scale Fluctuations of Human Prion Protein Determined by Restrained MD Simulations. *Biochemistry* **2011**, *50*, 10192−10194.
(47) Lane, T. J.; Bowman, G. R.; Beauchamp, K.; Voelz, V. A.; Pande, V. S. Markov State Model Reveals Folding and Functional Dynamics in Ultra-long MD Trajectories. *J. Am. Chem. Soc.* **2011**, *133*, 18413−18419.
(48) Shao, Q.; Yang, L.; Gao, Y. Q. Structure Change of β-hairpin Induced by Turn Optimization: An Enhanced Sampling Molecular Dynamics Simulation Study. *J. Chem. Phys.* **2011**, *135*, 235104.
(49) Zhuang, W.; Cui, R. Z.; Silva, D. A.; Huang, X. Simulating the T-Jump-Triggered Unfolding Dynamics of trpzip2 Peptide and Its Time-Resolved IR and Two-Dimensional IR Signals Using the Markov State Model Approach. *J. Phys. Chem. B* **2011**, *115*, 5415−5424.
(50) Haradaa, R.; Kitao, A. Multi-scale Free Energy Landscape Calculation Method by Combination of Coarse-grained and All-atom Models. *Chem. Phys. Lett.* **2011**, *503*, 145−152.
(51) Yang, L. J.; Shao, Q.; Gao, Y. Q. Thermodynamics and Folding Pathways of Trpzip2: An Accelerated Molecular Dynamics Simulation Study. *J. Phys. Chem. B* **2009**, *113*, 803−808.
(52) Noé, F.; Fischer, S. Transition Networks for Modeling the Kinetics of Conformational Change in Macromolecules. *Curr. Opin. Struct. Biol.* **2008**, *18*, 154−162.
(53) Chodera, J. D.; Singhal, N.; Pande, V. S.; Dill, K. A.; Swope, W. C. Automatic Discovery of Metastable States for the Construction of Markov Models of Macromolecular Conformational Dynamics. *J. Chem. Phys.* **2007**, *126*, 155101−155117.
(54) Bowman, G. R.; Huang, X.; Pande, V. S. Using Generalized Ensemble Simulations and Markov State Models to Identify Conformational States. *Methods* **2009**, *49*, 197−201.
(55) Buchete, N. V.; Hummer, G. Coarse Master Equations for Peptide Folding Dynamics. *J. Phys. Chem. B* **2008**, *112*, 6057−6069.
(56) Huang, X.; Yao, Y.; Bowman, G. R.; Sun, J.; Guibas, L. J.; Carlsson, G.; Pande, V. S. Constructing Multi-resolution Markov State Models (msms) to Elucidate RNA Hairpin Folding Mechanisms. *Pac. Symp. Biocomput.* **2010**, 228−239.
(57) Hsu, C.-P.; Flemming, G. R.; Head-Gordon, M.; Head-Gordon, T. *J. Chem. Phys.* **2001**, *114*, 3065.
(58) Gao, F.; Zhao, Y.; Liang, W. Z. *J. Phys. Chem. B* **2011**, *115*, 2699.
(59) Spano, F. C.; Clark, J.; Silva, C.; Friend, R. H. *J. Chem. Phys.* **2009**, *130*, 074904. Spano, F. C.; Meskers, S. C. J.; Hennebicq, E.; Beljonne, D. *J. Chem. Phys.* **2008**, *129*, 024704.
(60) von Dijk, L.; Bobbert, P. A.; Spano, F. C. *J. Phys. Chem. B* **2009**, *113*, 9708. von Dijk, L.; Bobbert, P. A.; Spano, F. C. *J. Phys. Chem. B* **2010**, *114*, 817.
(61) Seibt, J.; Marquetand, P.; Engel, V.; Chen, Z.; Dehm, V.; WÍźrthner, F. *Chem. Phys.* **2006**, *328*, 354. Seibt, J.; Engel, V. *Chem. Phys.* **2008**, *347*, 120. Seibt, J.; Dehm, V.; WÍźrthner, F.; Engel, V. *J. Chem. Phys.* **2008**, *128*, 204303.
(62) Zhao, Y.; Liang, W. Z.; Nakamura, H. Semiclassical Treatment of Thermally Activated Electron Transfer in the Intermediate to Strong Electronic Coupling Regime under the Fast Dielectric Relaxation. *J. Phys. Chem. A* **2006**, *110*, 8204−8212.
(63) (a) Dewar, M. J. S.; Zoebisch, E. G.; Healy, E. F.; Stewart, J. J. P. AM1: A New General Purpose Quantum Mechanical Model. *J. Am. Chem. Soc.* **1985**, *107*, 3902−3909. (b) Ponder, J. W.; Case, D. A. Force Fields for Protein Simulations. *Adv. Protein Chem.* **2003**, *66*, 27−85.

(64) Revision A.1 ; Frisch, M. J.; Trucks, G. W.; Schlegel, H. B.; Scuseria, G. E.; Robb, M. A.; Cheeseman, J. R.; Scalmani, G.; Barone, V.; Mennucci, B.; et al. *Gaussian 09*; Gaussian, Inc.: Wallingford, CT, 2009.
(65) Shao, Y.; Fusti-Molnar, L.; Jung, Y.; Kussmann, J.; Ochsenfeld, C.; Brown, S. T.; Gilbert, A. T. B.; Slipchenko, L. V.; Levchenko, S. V.; O'Neill, D. P.; et al. Advances in Methods and Algorithms in a Modern Quantum Chemistry Program Package. *Phys. Chem. Chem. Phys.* **2006**, *8*, 3172−3191.
(66) Becke, A. D. Density-functional Thermochemistry. III. The Role of Exact Exchange. *J. Chem. Phys.* **1993**, *98*, 5648−5652.
(67) Chai, J. D.; Head-Gordon, M. Systematic Optimization of Long-range Corrected Hybrid Density Functionals. *J. Chem. Phys.* **2008**, *128*, 084106.
(68) Rohrdanz, M. A.; Martins, K. M.; Herberta, J. M. A Long-range-corrected Density Functional that Performs Well for Both Ground-state Properties and Time-dependent Density Functional Theory Excitation Energies, including Charge-transfer Excited States. *J. Chem. Phys.* **2009**, *130*, 054112.
(69) (a) Roos, B. O.; Taylor, P. R.; Siegbahn, P. E. M. A Complete Active Space SCF Method (CASSCF) Using a Density Matrix Formulated Super-CI Approach. *Chem. Phys.* **1980**, *48*, 157−173. (b) Andersson, K.; Malmqvist, P.-Å.; Roos, B. O. Second-order Perturbation Theory with a Complete Active Space Self-consistent Field Reference Function. *J. Chem. Phys.* **1992**, *96*, 1218−1226.
(70) Serrano-Andrés, L.; Roos, B. O. Theoretical Study of the Absorption and Emission Spectra of Indole in the Gas Phase and in a Solvent. *J. Am. Chem. Soc.* **1996**, *118*, 185−195.
(71) (a) Dapprich, S.; Komaromi, I.; Byun, K. S.; Morokuma, K.; Frisch, M. J. A new ONIOM Implementation in Gaussian98. Part I. The Calculation of Energies, Gradients, Vibrational Frequencies and Electric Field Derivatives. *J. Mol. Struct.-THEOCHEM* **1999**, *461−462*, 1−21. (b) Vreven, T.; Morokuma, K. Hybrid methods: ONIOM-(QM:MM) and QM/MM. *Annu. Rep. Comput. Chem.* **2006**, *2*, 35−51.